Controlled Asymmetric Lamellar Nanomorphology Obtained through Nitroxide-Mediated Polymerization-Induced Microphase Separation

Laura García Andújar, Anne-Laure Brocas, Sylvain Bourrigaud, Sylvie Cazaumayou, Christophe Derail, Maud Save, Laurent Rubatat

Controlled Asymmetric Lamellar Nano-Morphology Obtained Through Nitroxide-Mediated Polymerization-Induced Microphase Separation

Laura García Andújar,[1,†] *Anne-Laure Brocas*,[2] *Sylvain Bourrigaud*,[2,‡] *Sylvie Cazaumayou*,[2] *Christophe Derail*,[1] *Maud Save*, [1] *Laurent Rubatat* [1,*]

[1] Universite de Pau et des Pays de l'Adour, E2S UPPA, CNRS, IPREM, Pau, France
[2] GRL, Arkema, B.P. 34, 64170 Lacq, France

TABLE OF CONTENT

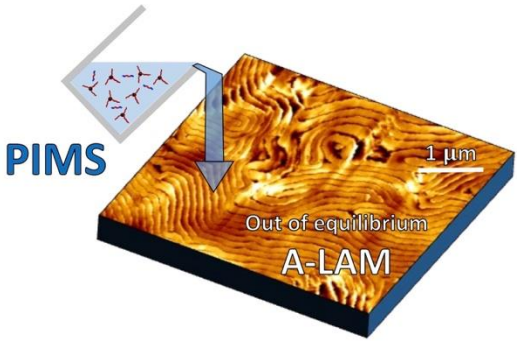

ABSTRACT

Polymerization-induced microphase separation (PIMS) is a rapid and efficient process to produce nanostructured polymers materials on large-scale. However, so far, it remains a challenge to produce well-defined morphologies with long-range ordering and controlled dimension. Herein we demonstrate that nitroxide-mediated PIMS can generate ordered asymmetric lamellar

morphologies of variable size over a long-range, by simple thermal dissociation of the first block. For that purpose, a low fraction (< 7.5 wt-%) of star poly(*n*-butyl acrylate-*co*-styrene) macroalkoxyamine (*s*-P(BA-*co*-S)-SG1), end functionalized with the SG1 nitroxide, was initially solubilized in methyl methacrylate monomer (MMA). The *s*-P(BA-*co*-S)-SG1 macroinitiator is thermally activated to be chain extended by bulk MMA nitroxide-mediated polymerization inducing simultaneous self-assembly of the *in situ* synthesized *s*-P(*n*BA-*co*-S)-*b*-PMMA block copolymer. This strategy produces asymmetric lamellar morphologies with large lamella period, up to 350 nm. The addition of varying fractions of a pre-synthetized PMMA-*b*-P*n*BA-*b*-PMMA triblock copolymer (from 0 to 16 wt-%) in the initial formulation is a key point to fine-tune the dimensions of the lamella periods from 350 nm down to 100 nm via a cosurfactant effect.

KEYWORDS

nanomorphology; polymerization-induced microphase separation; block copolymer; self-assembly; asymmetric lamellar.

INTRODUCTION

For decades, block copolymer (BCP) microphase segregation,[1-4] including BCP blended with homopolymers[5-9] or blends of BCPs,[10-12] have been intensively investigated and exploited to take advantage of the intrinsic block's properties. These studies demonstrated that a lamellar morphology is achieved primarily for balanced compositions of blocks at thermodynamic equilibrium; consequently, producing symmetric lamellae. Nevertheless, asymmetric lamellar morphologies (A-LAM) in nanostructured polymers are of great interest to produce materials with specific optical properties as photonic crystal (via control on the optical band gap),[13, 14] or

remarkable mechanical properties; e.g., associating high levels of stiffness and toughness (a soft minority phase combined to a hard majority phase).[15-17] Up to now, such A-LAM were achieved only with few systems at thermodynamical equilibrium. That includes BCPs with a bulky block, such as a hybrid polyhedral oligomeric silsesquioxane block,[18] or BCP composed of an intramolecularly crosslinked block coupled with a linear majority block.[19] BCP blends were also investigated, introducing the concept of cosurfactant effect.[20, 21] Hashimoto and Court reported A-LAM obtained with blends of high molar mass asymmetric linear diblock copolymer and low molar mass symmetric one.[20] Blends of homopolymer and miktoarm star BCP were reported as well, generating A-LAM which unbinds at large homopolymer content.[15, 22]

In the present work, we explore how polymerization-induced microphase separation (PIMS) process can be advantageous to produce straightforwardly A-LAM morphologies. Among the reaction-induced phase-transitions (RIPTs),[23] PIMS is an original, versatile and solvent free method to prepare out-of-equilibrium bulk nanostructured polymer materials in a single step.[24, 25] PIMS process involves polymerization of monomers in the presence of a reactive homopolymer in order to produce *in situ* block copolymer with two incompatible blocks self-assembling simultaneously to polymerization. One of the pioneer work in this field was dedicated to the synthesis of high-impact polystyrene from reactive polybutadiene dissolved in styrene monomer.[26] The bulk radical polymerization of styrene led to grafted copolymers *in situ* self-assembled into the so-call salami morphologies.[26] Later, bicontinous porous structures were obtained by bulk radical polymerization of styrene and divinylbenzene as crosslinker mediated by a polylactide (PLA) macromolecular chain transfer agent (macroCTA) to produce nanoporous materials after etching of the sacrificial PLA block.[27, 28] Most of the reported macroCTAs involved in PIMS present a linear architecture.[27-30] Nevertheless, multi-arm macroCTA were also reported in

photoactivated PIMS, highlighting their potential to generate original phase-inverted morphologies.[31] It is worth to note that well-defined morphologies with long-range ordering generated by PIMS are still scarce. Schulze and Hillmyer reported the occurrence of a LAM structure only with a crosslinker-free PIMS formulation.[32] Motokawa *et al.* reported the preparation of photonic crystals by PIMS.[33] Indeed they demonstrated that PIMS performed at temperature above the glass transition temperature (*Tg*) of all blocks, allows the self-assembly of large macromolecules into spherical domains with domain spacing up to 350 nm at full conversion. Interestingly, SANS monitoring during polymerization revealed transitory morphologies such as lamellar then cylinders with increasing degree of polymerization.[33, 34] Nevertheless, so far, stabilized and well-defined A-LAM morphologies, have never been achieved by PIMS process at full conversion.

To date, in PIMS involving radical polymerization, the reactive homopolymers were exclusively macroCTA synthesized by reversible addition fragmentation transfer (RAFT) polymerization.[29, 30] Among the reversible deactivation radical polymerization (RDRP) methods producing effective precursor of block copolymers, nitroxide-mediated polymerization (NMP) is attractive from its intrinsic mechanism based on reversible termination reaction instead of reversible transfer reactions involved in RAFT polymerization. Indeed, RAFT polymerization requires the addition of a molecular initiator to produce radicals from macroCTAs, which inherently produces a small fraction of homopolymer concomitantly to block copolymer. Interestingly NMP produces block copolymers by thermal dissociation of the macroalkoxyamine able to initiate the polymerization of the second monomer. The only study taking profit of NMP to design nanostructured materials by polymerization-induced phase separation (PIPS) dealt with the one step synthesis of amphiphilic gradient copolymers able to self-assemble into short-range ill-defined nanodomains

of 20 to 150 nm.[35] Up to now, macroalkoxyamines synthesized by NMP have never been investigated in PIMS.

Herein, we implemented a tailored PIMS approach involving a poly(*n*-butyl acrylate-*co*-styrene) reactive star macroalkoxyamine synthesized by NMP. The aim is to generate out-of-equilibrium asymmetric lamellar morphologies composed of poly(methyl methacrylate) (PMMA) as high *Tg* majority phase and poly(*n*-butyl acrylate-*co*-styrene) as minority soft phase. Indeed, the introduction of low *Tg* poly(*n*-butyl acrylate-*co*-styrene) nano-domains is known to improve the impact toughness properties of the glassy poly(methyl methacrylate) matrix at room temperature, while maintaining transparency by matching the refractive indexes.[36, 37] In addition, this strategy allows to produce the hard blocks on the BCP periphery favoring material's toughness,[17, 38, 39] and the final A-LAM morphology confers a high level of stiffness.[15-17] Moreover acrylic copolymers have demonstrated a superior oxidation and resistance to hydrocarbons compared to the more widely used styrene/isoprene/butadiene copolymers.[40] The main originality of the present work is to drive the PIMS process through a cosurfactant effect using a pre-synthesized PMMA-*b*-P*n*BA-*b*-PMMA linear triblock copolymer (named TBCP) added at the initial stage of polymerization together with the reactive *s*-P(*n*BA-*co*-S)-SG1 star macroinitiator and MMA monomer. We explore the feasibility of chain extending the soft block while maintaining the LAM structure and controlling the LAM period by varying the content of TBCP additive.

MATERIALS & METHODS

Materials. Methyl methacrylate (MMA) was provided by Arkema. Bis(2,2,6,6,-tetramethyl-4-piperidyl)sebaceate (Tinuvin 770) and 2-(2H-benzotriazol-2-yl)-p-cresol (Tinuvin P) light stabilizers were provided by Arkema. 1,1′-Azobis(cyclohexanecarbonitrile) (VAZO-88, 98 %)

was supplied from Sigma-Aldrich. Arkema provided the *s*-P(*n*BA-*co*-S)-SG1 star poly(*n*-butyl acrylate-*co*-styrene) used in this study as reactive first block in PIMS process. The *s*-P(*n*BA-*co*-S)-SG1 macroalkoxyamine was synthesized by nitroxide-mediated copolymerization (NMP) of *n*-butyl acrylate (*n*BA) and styrene (S) in bulk at 115 °C from the trifunctional alkoxyamine developed by Arkema (see Scheme 1). The final composition of *s*-P(*n*BA-*co*-S)-SG1 determined by ^{1}H NMR (Figure S1), is 81 wt-% in *n*BA and 19 wt-% in S. The number-average molar mass of *s*-P(*n*BA-*co*-S)-SG1, determined by SEC-MALLS (see characterization methods below) is M_n = 230 060 g mol^{-1} with dispersity $Đ$ = 1.6 by using a *dn/dC* value of 0.096 (see Figure S6a for *dn/dC*). Figure S4 displays the SEC chromatogram recorded from Astra software. Figure S7 displays the DSC trace collected on *s*-P(*n*BA-*co*-S)-SG1 and the evaluation of its *Tg* at -19 °C. The poly(methyl methacrylate)-*b*-poly(*n*-butyl acrylate)-*b*-poly(methyl methacrylate) pre-formed triblock copolymer (named TBCP) was supplied by Arkema and synthesized by NMP at 115 °C. The final composition of TBCP determined by ^{1}H NMR is 47 wt-% in *n*BA ($W_{n\mathrm{BA}}$ = 0.47) and 53 wt-% in MMA (W_{MMA} = 0.53). The number-average molar mass determined by SEC-MALLS of TBCP is M_n = 50 890 g mol^{-1} with dispersity $Đ$ = 1.5 by using a *dn/dC* value of 0.082 (see Figure S6b for *dn/dC*). The raw SEC chromatogram recorded from Astra software is displayed in Figure S5.

Preparation of nanostructured polymer by PIMS process. The initial liquid formulations are prepared in an Erlenmeyer flask. *s*-P(*n*BA-*co*-S)-SG1 star macroalkoxyamine, PMMA-*b*-P*n*BA-*b*-PMMA triblock copolymer (TBCP), Tinuvin® light stabilizer (1000 ppm, 50/50 w/w Tinuvin P/Tinuvin 770) and 1,1′-Azobis(cyclohexanecarbonitrile) VAZO-88 (735 ppm) post-initiator are first dissolved in MMA. The weight ratio of MMA monomer over *s*-P(*n*BA-*co*-S)-SG1 star macroalkoxyamine was set constant at a value of 12.3, in order to target the same molar mass of

the *in situ* formed star block copolymer (*s*-BCP) (see Table S1). The initial weight fraction of *s*-P(*n*BA-*co*-S)-SG1, based on the total weight of formulation, was tuned from 6.3 to 7.5 wt-% (see Table 1). Oxygen from air is removed by vacuum cycles during 30 min. The formulations were introduced between two glass windows (25 × 25 cm^2) separated by an elastomeric spacer of 3 mm, altogether tightened with clamps. The bulk polymerization was performed in an oven. The temperature ramp was initially optimized to avoid material defects (*e.g.*, bubbles) and to reach the highest final MMA conversion ranging between 96.8 and 99.5 % (see Table S2 and Figure S9). A first temperature ramp is applied, from 20 °C to 75 °C for 50 minutes followed by a second heating ramp from 75 °C to 85 °C for 520 minutes. A third heating ramp from 85 °C to 125 °C for 430 minutes was applied. The final polymerization cycle aims at activating the VAZO-88 post-initiator for 60 minutes at 125 °C to polymerize residual MMA monomer. After polymerization, the polymer sheets were easily separated from both glass windows and solid aliquots were collected for the characterizations.

Size exclusion chromatography (SEC). The number-average molar mass (M_n) and dispersity ($Đ$) of samples were determined by size exclusion chromatography (SEC) at 30 °C with tetrahydrofuran (THF) as eluent at a flow rate of 1 mL min^{-1}. All polymer samples were prepared at 0.1 to 0.3 g L^{-1} concentrations and filtered through PTFE 0.45 mm filters. The SEC was equipped with a Viscotek-Malvern VE isocratic pump, Viscotek-Malvern VE 1122 automatic injector, Shodex columns (KF 803L, KF 804L, KF 806L, 8 × 300 mm), a VE 7510 Viscotek solvent degasser and different detectors working in series: a Heleos II Multi Angle Laser Light Scattering detector (MALLS, 18 angles, λ_0 = 664.4 nm, Wyatt Technology), a ViscoStar (Wyatt Technology) viscosimeter and a Viscotek-Malvern VE 3580 refractive index (RI) detector. The refractive index increments (*dn/dC*) of *s*-P(*n*BA-*co*-S)-SG1 macroalkoxyamine and pre-formed TBCP were

measured in THF at 30 °C with an Optilab T-rex refractometer from Wyatt technology working at λ = 658 nm wavelength. *dn/dC* values are extracted from the slope of refractive index of the constant plateau value versus concentration on Astra Software (Figure S6).

Proton Nuclear Magnetic Resonance (NMR). The ^{1}H NMR spectra of the copolymers were recorded at 25 °C in a Bruker Advanced AM400 spectrometer (400 MHz) using $CDCl_3$ as deuterated solvent.

Differential scanning calorimetry (DSC). A TA Instruments DSC-100 apparatus was used to determine glass transition temperatures, *Tg*. Approximately 10 mg of sample was poured in hermetic aluminum pans and then exposed to temperatures ranging from -80 to 150 °C under an air flow of 50 mL min^{-1}.

Atomic Force Microscopy (AFM). The AFM samples are prepared by ultramicrotomy at room temperature with a Leica EM UC7. First, they are trimed with a Diatome® diamond knife Cryotrim 45°, then the final surfaces are obtained with a Diatome® diamond Ultra 45 knife targeting thickness of 50 nm. AFM topographic images are collected with a MultiMode 8 from Bruker using PeakForce QNM (Quantitative NanoMechanics) mode at room temperature. The ScanAsyst-Air mode is used with a V-shaped silicon nitride cantilever presenting a nominal tip radius of 25 nm and a spring constant of 0.40 N m^{-1}. Image analysis is performed using NanoScope Analysis version 1.5 software; the characteristic dimensions are extracted using the section tool.

Small Angle X-ray Scattering (SAXS). The SAXS data, from Figure 1 and Figure 3, were collected on the SWING beamline at SOLEIL synchrotron (Saclays, France). The X-ray wavelength, λ, used is 1.77 Å, with a sample-to-detector distance of 6.598 m. The spectra collected on sample containing 10 wt-% of tri-BCP is performed with a sample-to-detector distance of 3.998 m. The

SAXS data, from Figure S10, were collected on the BL11-NCD-SWEET beamline at ALBA synchrotron (Barcelona, Spain). The X-ray wavelength, λ, used is 1.179 Å, with a sample-to-detector distance of 1.943 m. The standard data treatment is performed and the scattering curves are plotted as *I(q)* where *I* is the scattering intensity in arbitrary units and *q* the scattering vector in $Å^{-1}$, as $q=4\pi/\lambda.sin(\theta/2)$, θ being the scattering angle. The data are all collected at room temperature.

Dynamical Mechanical Thermal Analysis (DMTA). The measurements were performed with an ARES rheometer (TA Instrument, AR 2000) operating under controlled-stress. The geometry used was rectangular solid samples sawn in the polymer sheets with dimensions 45 mm × 10 mm × 3 mm. A stress sweep was systematically performed before each experiment to ensure working in the linear domain. *G'* storage modulus and *G''* loss modulus were collected at a fixed circular frequency of 1 Hz as function of temperature, from -50 to 180 °C with a ramp of 1 °C min^{-1}. $Tan\delta$ curves were obtained by dividing *G''* by *G'*, and glassy transition temperatures, $T\alpha$, corresponds to $Tan\delta$ peaks.

RESULTS AND DISCUSSION

The *s*-P(*n*BA-*co*-S)-SG1 reactive macroalkoxyamine, synthesized by bulk NMP from a trifunctional alkoxyamine, presents a final composition of 81 wt-% in *n*BA and 19 wt-% in S (Figure S1). This composition was set to match the refractive index of PMMA to achieve the best transparency of the final material. The star *s*-P(*n*BA-*co*-S)-SG1 was solubilized in MMA monomer to further act as macroinitiator of bulk MMA polymerization upon heating and dissociating the macroalkoxyamine, as depicted on Scheme 1. The temperature ramp detailed in experimental part, and in Figure S9, starts below *Tg* of PMMA (114 °C, Figure S8) for 880 minutes, then slightly above this *Tg* for about 180 minutes. This temperature ramp was optimized to produce transparent

and defect-free PMMA-based sheet (Figure S11) while targeting high MMA conversion (Table S2). Table 1 presents the series of samples synthesized by PIMS with various fractions of pre-formed TBCP. The reference polymer, resulting from the bulk MMA polymerization of the formulation containing solely 7.5 wt-% of *s*-P(*n*BA-*co*-S)-SG1 star macroalkoxyamine in the absence of TBCP is named *s*-BCP (Table 1). The number-average molar mass of the *s*-BCP sample is equal to 9.83×10^5 g mol^{-1} and the dispersity of the monomodal SEC chromatogram is 1.5 (Figure 2f). Note that the clear shift of the SEC chromatogram towards higher molar masses compared to the initial of *s*-P(*n*BA-*co*-S)-SG1 macroalkoxyamine confirms the successful chain extension by MMA polymerization (Figure S12).

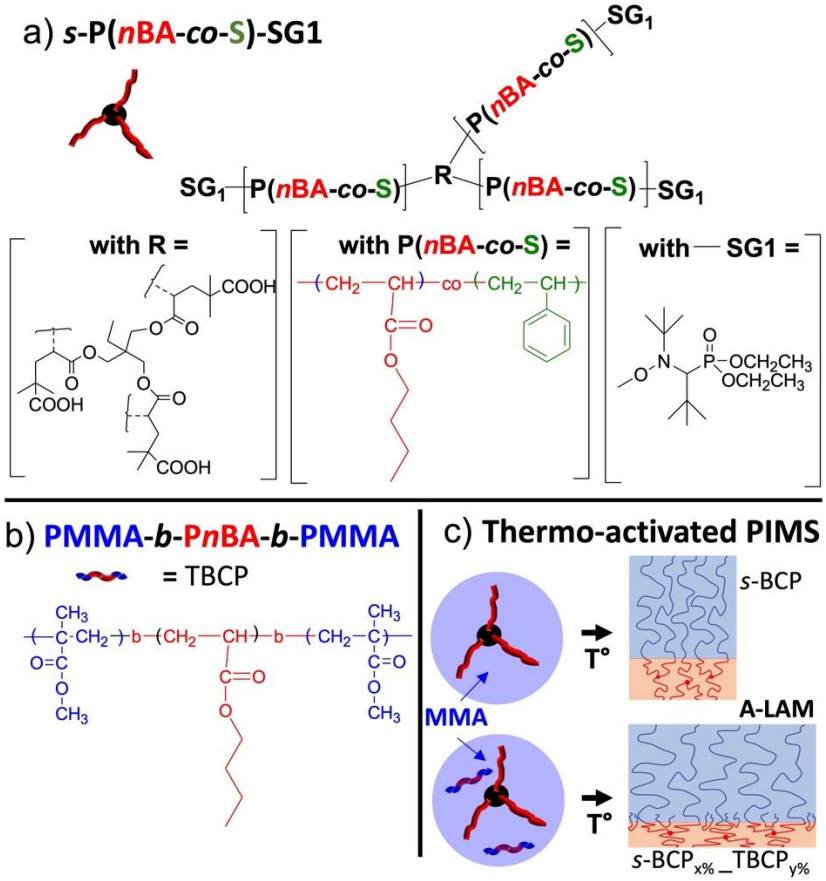

Scheme 1. Structure of (a) the *s*-P(*n*BA-*co*-S)-SG1 star macroalkoxyamine and (b) of the PMMA-*b*-P*n*BA-*b*-PMMA pre-synthesized triblock copolymer (TBCP). (c) Hypothesized schemes depicting the blocks arrangement at the lamellar interfaces for *s*-BCP sample and *s*-BCP_TBCP sample (with additional triblock copolymer). The red and blue segments correspond respectively to the P(*n*BA-*co*-S)-SG1 star macroinitiator and the PMMA blocks.

Table 1. Initial composition of formulations synthesized by PIMS in bulk.

	Initial composition		
Samples	$W_{s\text{-P}(n\text{BA-}co\text{-S})\text{-SG1},0}$ **(wt-%)**[a]	$W_{\text{TBCP},0}$ **(wt-%)**[a]	$W_{\text{MMA},0}$ **(wt-%)**[a]
s-BCP	7.5	0	92.1
$s\text{-BCP}_{97.5\%}\_\text{TBCP}_{2.5\%}$	7.3	2.5	89.7
$s\text{-BCP}_{95\%}\_\text{TBCP}_{5\%}$	7.1	5.0	87.3
$s\text{-BCP}_{90\%}\_\text{TBCP}_{10\%}$	6.8	10.0	83.6
$s\text{-BCP}_{84\%}\_\text{TBCP}_{16\%}$	6.3	16.0	76.9

[a] Initial weight fractions of *s*-P(*n*BA-*co*-S)-SG1, or TBCP, or MMA based on the total formulation including MMA, *s*-P(*n*BA-*co*-S)-SG1, TBCP but also Tinuvin and VAZO-88 additives (see Table S1).

Figure 1a displays a representative topographic AFM images collected on the ultramicrotomed *s*-BCP sample with a clear phase segregation. Despite the low fraction of soft P*n*BA rich phase, i.e.,

7.5 wt-%, PIMS produced well-defined lamellar structures, consequently highly asymmetrical. The long-range ordering was corroborated by Small Angle X-ray Scattering (SAXS) with sequences of structural factor peaks at q^*, $2q^*$, $3q^*$ and $4q^*$; where q^* is the first order peak (Figure 1b). A large averaged lamellar period of 350 nm was calculated from Eq 1.

$$d_{Lam}=2\pi/q^* \qquad \textbf{Eq 1.}$$

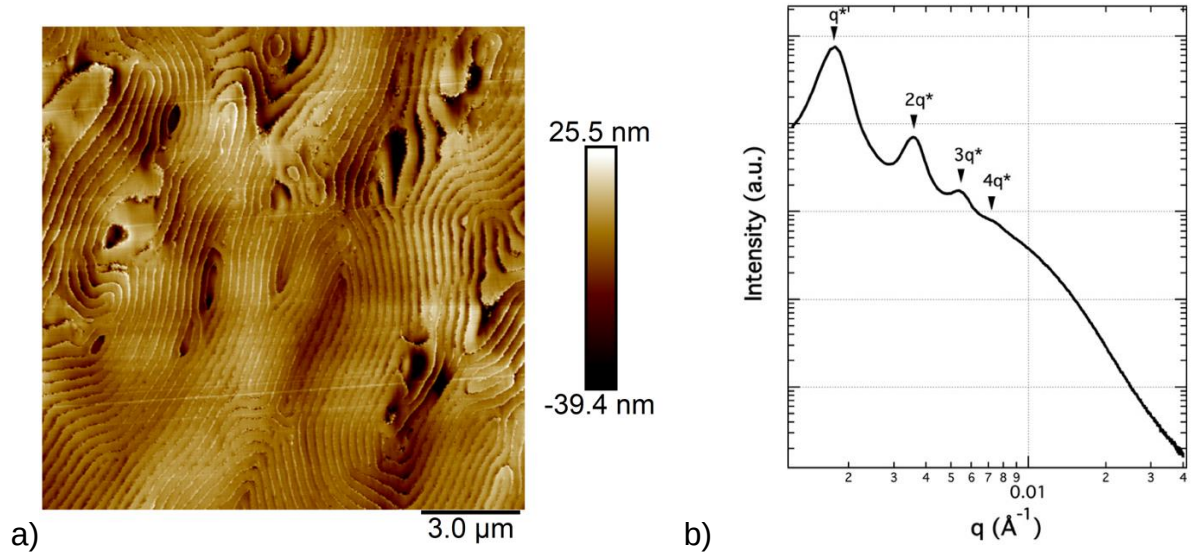

Figure 1. a) AFM height image of *s*-BCP with the thinner dark phase assigned to P(*n*BA-*co*-S) and the thicker bright lamellae to PMMA rich domains. b) SAXS data of *s*-BCP with peak's assignments.

The occurrence of that LAM morphology can be discussed on the basis of the concomitant self-assembly and macromolecular mobility decrease with monomer conversion leading to a kinetically trapped structure. Motokawa *et al.* have observed with a linear macroCTA, at a polymerization temperature higher than both block *Tg*, that the initial morphology is lamellar. Then the growing macromolecules maintain enough mobility to switch to cylindrical and spherical morphologies.[33] In our system, the initial LAM self-assembly is reached, but then due to temperatures below PMMA *Tg* during the major part of the PIMS process (Figure S9), the lack of macromolecular

mobility does not allow further transitions. Nonetheless, the MMA polymerization is pursued while keeping the lamellar morphology mostly unchanged. It is interesting to note that, at equilibrium, the mean-field theory does not predict LAM structure but a mixed state for star BCPs with such a large volume fraction of outer blocks (ca. 87 vol-%).[41] This indicates that the limited exposition to temperature above PMMA *Tg* during PIMS process does not induce the sufficient macromolecular mobility required to reach equilibrium. Note that the choice of a star *s*-P(*n*BA-*co*-S)-SG1 macroalkoxyamine was driven by preliminary results investigating PIMS mediated by either a monofunctional or a difunctional macroalkoxyamines (Table S3, Table S4 and Figure S13). None of those additional formulations produced LAM morphologies. Thus, the star architecture and high molar mass of the *s*-P(*n*BA-*co*-S)-SG1 are key points to limit the chain mobility. Also, formulations with other *s*-P(*n*BA-*co*-S)-SG1 contents, i.e., 3.5 and 15 wt-%, were investigated. None of them generated LAM structure (Table S5, and Figure S14). This evidences the narrow composition window to produce A-LAM by PIMS.

In order to drive the lamellae dimensions produced by PIMS, the strategy proposed in the present work is to add a low fraction of a pre-synthetized PMMA-*b*-P*n*BA-*b*-PMMA linear triblock copolymer (TBCP) to the initial *s*-BCP formulation (Table 1). This TBCP pre-formed triblock copolymer synthesized by NMP was composed of 47 wt-% of P*n*BA and 53 wt-% of PMMA and of number-average molar mass M_n = 50 890 g mol^{-1} and dispersity of $Đ$ = 1.5 (Table 2, Figure S5). Different samples were thus prepared by PIMS with a constant weight ratio MMA monomer over *s*-P(*n*BA-*co*-S)-SG1 macroinitiator equal to 12.3 (see Table S1). On the other hand, the fraction of TBCP ranged from 2.5 to 16 wt-% based on the total weight of the formulation (Table 1). The final PIMS samples containing *in situ* synthesized *s*-BCP and pre-formed TBCP were analyzed by size exclusion chromatography (Figure 2f and Figure S15). Monomodal SEC chromatograms were

recovered (Figure 2f) and the M_n values of the blends decreased by increasing the TBCP fraction along with an increase of the dispersity value as reported in (Table 2). That was expected for blends of high molar mass star block copolymers with an increasing fraction of lower M_n triblock copolymer (see Figure S15a). It is worth to note that the experimental sample's M_n values are in good agreement with the corresponding theoretical M_n, calculated from the molar fractions of *s*-BCP and TBCP (see supporting information and Table S6). Also, it should be noted that the conformation plots ($R_g \propto M^{\alpha}$) of *s*-BCP and *s*-BCP_TBCP samples corroborate the synthesis of star block copolymers by PIMS process as the low values of the slope (α exponent ~ 0.4, see Figure S15b) indicates higher compaction of branched macromolecules.[42]

Table 2. Final polymer sample characteristics.

	Final samples				
Samples	$W_{PMMA,exp.}$ **(wt-%)** [a]	$V_{PMMA,exp.}$ ***(vol-%)*** [b]	M_n **(g mol^{-1})** [c]	$Đ$	d_{LAM} **(nm)** [d]
s-BCP	87.8	87	9.83×10^5	1.5	350
s-BCP$_{97.5\%}$_TBCP$_{2.5\%}$	87.7	87	6.68×10^5	1.6	260
s-BCP$_{95\%}$_TBCP$_{5\%}$	81.8	80	5.30×10^5	1.7	180
s-BCP$_{90\%}$_TBCP$_{10\%}$	80.4	79	3.02×10^5	2.1	110
s-BCP$_{84\%}$_TBCP$_{16\%}$	77.7	76	2.92×10^5	2.3	92
TBCP	53	51	5.089×10^4	1.5	23.3

[a] Final weight fraction of PMMA determined by ^{1}H NMR analysis of the final polymer sample (Figure S2 and Figure S3).
[b] Final volume fraction of PMMA estimated from $W_{PMMA,exp.}$ and polymer densities (ρ_{PMMA} = 1.18 g cm^{-3}, ρ_{PnBA} = 1.08 g cm^{-3} and ρ_{PS} = 1.04 g cm^{-3}).
[c] Number-average molar mass determined by SEC equipped with online refractometer and multi-angle laser light scattering detector (MALLS) (see Figure 2f, Figure S6 and Figure S15).
[d] Lamellar period obtained by SAXS (see Eq 1).

Topographic AFM images collected on the ultramicrotomed samples are presented in Figure 2. As for the pure *s*-BCP sample, all samples with added pre-formed TBCP present a phase segregation

with well-defined lamellar structures. A-LAM morphologies were also observed at low TBCP contents of 2.5, 5 and 10 wt-%. SAXS analyses corroborated the morphologies observed by AFM. The scattering curves collected on *s*-$BCP_{97.5\%}$_$TBCP_{2.5\%}$, *s*-$BCP_{95\%}$_$TBCP_{5\%}$ and *s*-$BCP_{90\%}$_$TBCP_{10\%}$ samples show unambiguously lamellar structures and a high degree of ordering, with sequences of higher order peaks at *q**, *2q**, *3q** and *4q** (Figure 3). On the other hand, AFM image collected on sample *s*-$BCP_{84\%}$_$TBCP_{16\%}$ presents short lamellae with a lower degree of ordering confirmed also by SAXS with broader peaks and a reduced sequence of orders (*q**, *2q** and *3q**). The observed phase separation is also pointed out by the dynamical mechanical thermal analysis (DMTA) (see supporting information, Figure S16). Indeed, two well separated mechanical glass transition temperatures, $T\alpha$, are systematically identified at tanδ curves maxima. $T\alpha$ ranging from -20 to -10 °C is associated to macroinitiator rich domains and $T\alpha$ ranging from 120 to 130 °C to the PMMA rich ones.

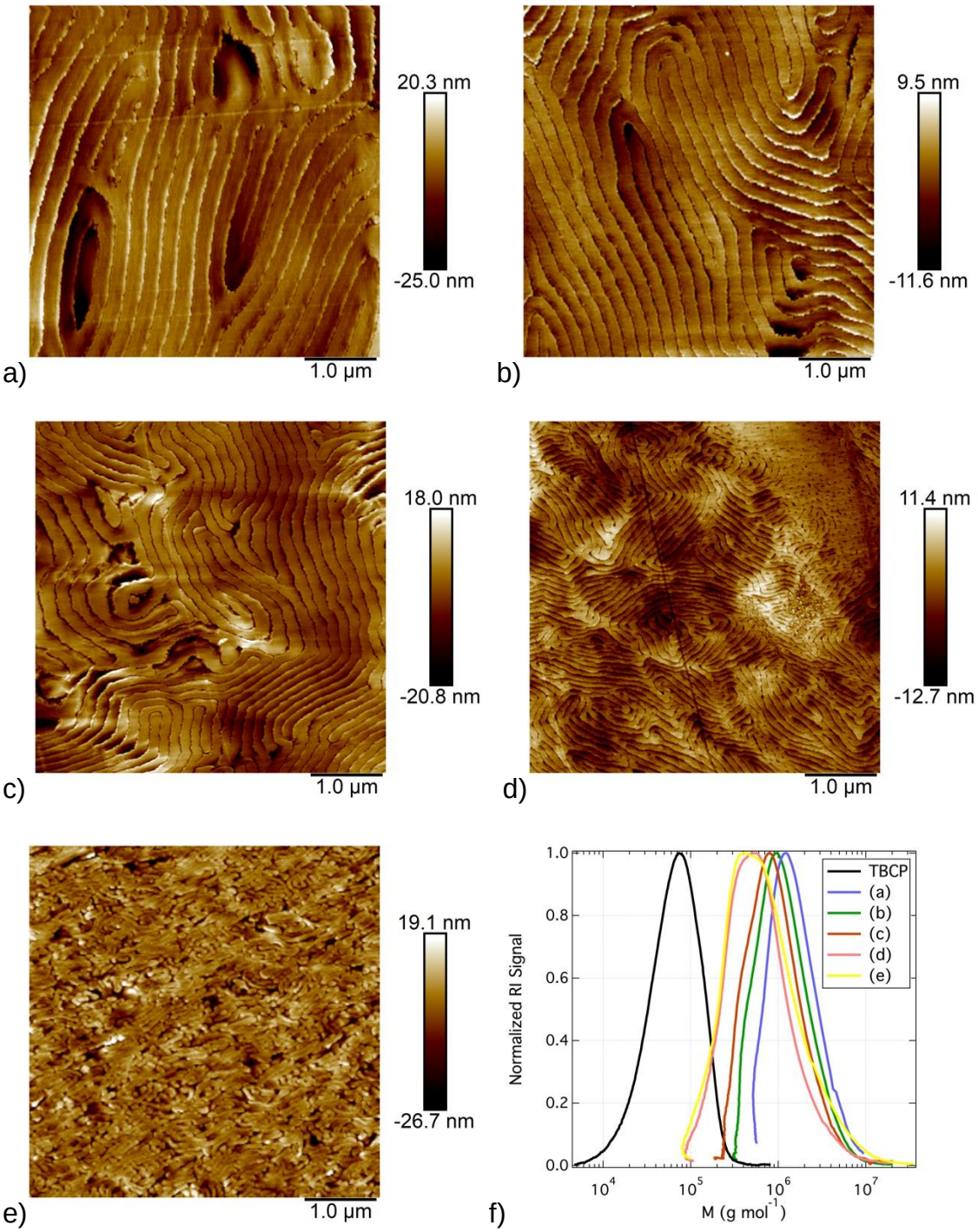

Figure 2. AFM height images collected on (a) *s*-BCP sample and samples synthesized from *s*-P(*n*BA-*co*-S)-SG1 with different amounts of added TBCP: (b) *s*-BCP$_{97.5\%}$_TBCP$_{2.5\%}$, (c) *s*-BCP$_{95\%}$_TBCP$_{5\%}$, (d) *s*-BCP$_{90\%}$_TBCP$_{10\%}$, (e) *s*-BCP$_{84\%}$_TBCP$_{16\%}$. (f) Overlay of SEC chromatograms, normalized RI signal versus molar mass, of TBCP (black) and (a), (b), (c), (d) and (e) *s*-BCP and *s*-BCP_TBCP samples.

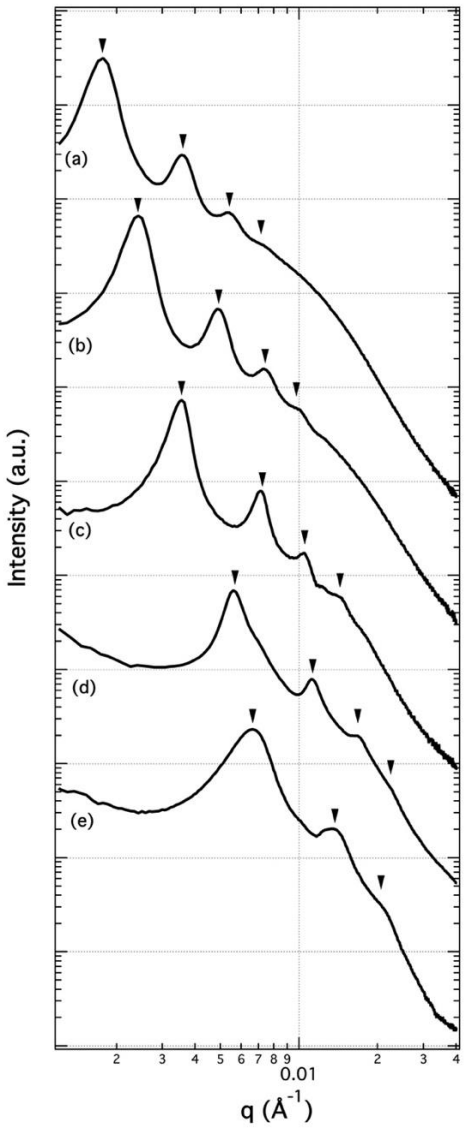

Figure 3. SAXS spectra collected on (a) *s*-BCP sample and samples synthesized from *s*-P(*n*BA-*co*-S)-SG1with different amounts of added TBCP: (b) *s*-$BCP_{97.5\%}$_$TBCP_{2.5\%}$, (c) *s*-$BCP_{95\%}$_$TBCP_{5\%}$, (d) *s*-$BCP_{90\%}$_$TBCP_{10\%}$, (e) *s*-$BCP_{84\%}$_$TBCP_{16\%}$. The arrows correspond to the lamellar peak positions in the order: *q**, *2q**, *3q** and *4q**. The scattering curves are shifted vertically for sake of clarity.

Interestingly, both AFM and SAXS analyses highlighted that increasing the amount of TBCP from 2.5 to 16 wt-% induced a decrease of the lamellar period from 350 to 92 nm (Figure 2 and Figure 3), as calculated from the *q* values of the main structural peak (Table 2). It can be noted that within the explored polymer fraction range, no macro-phase separation was observed, indicating a good

compatibility between the pre-formed PMMA-*b*-P*n*BA-*b*-PMMA triblock copolymer and the *in situ* synthesized *s*-BCP star block copolymer. Consequently, the added TBCP should preferentially be located at the interface between both P(*n*BA-*co*-S) and PMMA phases, acting as a cosurfactant during PIMS process. This mechanism has been already described for blends of diblock copolymers at thermodynamical equilibrium.[20, 27, 43, 44] In order to accommodate the TBCP, the averaged distance between the star branch ends at the interphases should be increased compared to the neat *s*-BCP sample. This leads to star branches stretching along the P*n*BA rich lamellae and to a decrease of its thickness, as depicted on Scheme 1c. Consequently, the larger area per branch generated at the interphase explain the thinner PMMA lamellae thicknesses at full conversion.

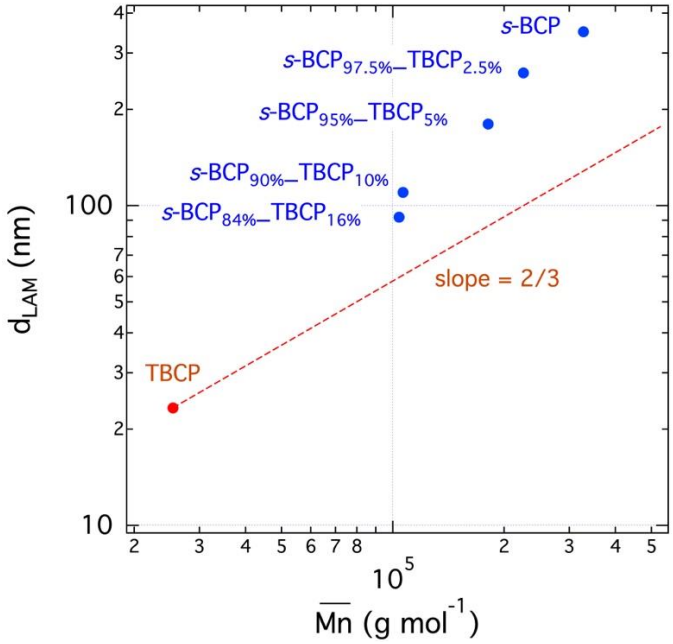

Figure 4. (Blue markers) Experimental lamellae-to-lamellae period in PIMS samples, d_{LAM} (Table 2), versus $M_{n.exp\ arm}$ of each P(*n*BA-*co*-S)-*b*-PMMA arm (Table S6 and Eq S9). (Red marker) Experimental lamellae-to-lamellae period d_{LAM} in the TBCP copolymer (Table 2). (Red line) theoretical 2/3 power law intercepting the red TBCP marker.

The dependency of lamellar *d*-spacing on copolymer M_n was extensively studied for linear BCP at thermodynamical equilibrium, with a predicted 2/3 power-law,[45, 46] also observed

experimentaly.[47] A quasi similar dependence was observed for star BCP with a 0.68 power law, while considering the M_n of a single branch.[48] Regarding BCP blends, Hashimoto *et al.* reported that the *d*-spacing versus the averaged M_n of the overall linear BCP blends followed also the 2/3 power-law.[44, 49] Figure 4 presents the PIMS lamellar *d*-spacing, $d_{LAM,}$ calculated from the SAXS data versus the averaged arm's M_n, estimated from the experimental blend M_n as described in supporting information (Table S6). As a reference, a 2/3 power law intercepting the experimental point corresponding to the TBCP measured at thermodynamical equilibrium is plotted. Interestingly, the experimental values of *s*-BCP_TBCP samples are all located above the 2/3 power law reference curve and approach it with increasing TBCP content (Figure 4). Such high values of lamellae-to-lamellae period might indicate an excess of chain stretching in the kinetically trapped morphology compared to the equilibrium state. This effect is particularly pronounced for *s*-BCP sample and it is reduced by increasing the initial TBCP content. This trend is well in agreement with the cosurfactant effect of TBCP inducing an increase of the interfacial area per branch.

CONCLUSION

Nanostructured block copolymer materials made of poly(methyl methacrylate) as high glass transition temperature majority phase and a soft poly(*n*-butyl acrylate)-based minority phase were successfully synthesized by applying nitroxide-mediated polymerization (NMP) to the concept of polymerization-induced microphase separation (PIMS) process. Characterization of macromolecular features and nano-morphologies confirmed the successful synthesis of block copolymers via *in situ* chain extension of the poly(*n*-butyl acrylate-*co*-styrene)-SG1 star macroalkoxyamine by quantitative bulk polymerization of MMA. The present study highlights that well-controlled lamellar morphologies, including asymmetric lamellar morphologies with a

long-range ordering, can be achieved straightforwardly by NMP PIMS process. Interestingly, a cosurfactant effect brought by a pre-synthetized PMMA-*b*-P*n*BA-*b*-PMMA triblock copolymer inserted at the initial stage of PIMS process is a key point to control the dimension of the lamellae periods from 350 nm down to 100 nm. This study paves the way for further developing a diversity of long range ordered morphologies mastered by *in situ* SAXS monitoring of the NMP PIMS process.

SUPPORTING INFORMATION CONTENT

Molar and weight fractions in *s*-P(*n*BA-*co*-S)-SG1 and *s*-BCP_TBCP samples; Analysis of *s*-P(*n*BA-*co*-S)-SG1 and TBCP by size exclusion chromatography in THF; Refractive index increment (*dn/dC*) of *s*-P(*n*BA-*co*-S)-SG1 and TBCP; Differential scanning calorimetry of *s*-P(*n*BA-*co*-S)-SG1 and *s*-BCP; Preparation of PIMS formulations and monomer conversions; PIMS temperature ramp; Morphological characterization of TBCP; Transparency of *s*-BCP sample; Overlay of *s*-P(*n*BA-*co*-S)-SG1 and *s*-BCP chromatograms; Impact of macroalkoxyamine functionality; Impact of *s*-P(*n*BA-*co*-S)-SG1 content in the formulation; Analysis of *s*-BCP_TBCP samples by size exclusion chromatography in THF; Rheological properties of *s*-BCP and *s*-BCP_TBCP samples.

AUTHOR INFORMATION

Corresponding Author

E-mail: laurent.rubatat@univ-pau.fr

Present Addresses

† Saint Gobain Recherche Paris, Quai Lucien Lefranc, 93303 Aubervilliers Cedex, France

‡ M2i, Chemstart'up pôle 2, Allée Le Corbusier, 64170 Lacq, France.

Author Contributions

All authors have given approval to the final version of the manuscript.

Funding Sources

This work benefited from the financial support of Region Nouvelle Aquitaine (France), (MAHE Project). LGA, MS, CD and LR thank Arkema for the financial support and for providing Flexibloc® macroalkoxyamine and the triblock copolymer.

ACKNOWLEDGEMENT

The authors thanks Region Nouvelle Aquitaine (France) and Arkema for funding. V. Pellerin, A. Khoukh, G. Lahittète, G. Penacq and V. Carrère for they help on analysis and laboratory support at IPREM and Arkema. We acknowledge SOLEIL for provision of synchrotron radiation facilities and we would like to thank J. Perez and T. Bizien for assistance in using beamline SWING. We acknowledge ALBA synchrotron for provision of beamtime on BL11 NCD-SWEET beamline; M. Malfois and X. Pascassio-Comte are thanked for their assistance in data collection. I. Iliopoulos, B. Charrière and O. Borisov are thanked for the fruitful discussions during the project and the writing process.

REFERENCES

1. Rosedale, J. H.; Bates, F. S., Rheology of ordered and disordered symmetric poly(ethylenepropylene)-poly(ethylethylene) diblock copolymers. *Macromolecules* **1990,** *23* (8), 2329-2338.

2. Schulz, M. F.; Khandpur, A. K.; Bates, F. S.; Almdal, K.; Mortensen, K.; Hajduk, D. A.; Gruner, S. M., Phase Behavior of Polystyrene−Poly(2-vinylpyridine) Diblock Copolymers. *Macromolecules* **1996,** *29* (8), 2857-2867.

3. Matsen, M. W.; Thompson, R. B., Equilibrium behavior of symmetric ABA triblock copolymer melts. *The Journal of Chemical Physics* **1999,** *111* (15), 7139-7146.

4. Matsushita, Y.; Noro, A.; Iinuma, M.; Suzuki, J.; Ohtani, H.; Takano, A., Effect of Composition Distribution on Microphase-Separated Structure from Diblock Copolymers. *Macromolecules* **2003,** *36* (21), 8074-8077.

5. Kinning, D. J.; Winey, K. I.; Thomas, E. L., Structural transitions from spherical to nonspherical micelles in blends of poly(styrene-butadiene) diblock copolymer and polystyrene homopolymers. *Macromolecules* **1988,** *21* (12), 3502-3506.

6. Tanaka, H.; Hasegawa, H.; Hashimoto, T., Ordered structure in mixtures of a block copolymer and homopolymers. 1. Solubilization of low molecular weight homopolymers. *Macromolecules* **1991,** *24* (1), 240-251.

7. Kinning, D. J.; Thomas, E. L.; Fetters, L. J., Morphological studies of micelle formation in block copolymer/homopolymer blends: comparison with theory. *Macromolecules* **1991,** *24* (13), 3893-3900.

8. Matsen, M. W., Phase Behavior of Block Copolymer/Homopolymer Blends. *Macromolecules* **1995,** *28* (17), 5765-5773.

9. Shi, W.; Li, W.; Delaney, K. T.; Fredrickson, G. H.; Kramer, E. J.; Ntaras, C.; Avgeropoulos, A.; Lynd, N. A., Morphology re-entry in asymmetric PS-PI-PS' triblock

copolymer and PS homopolymer blends. *Journal of Polymer Science Part B: Polymer Physics* **2016,** *54* (2), 169-179.

10. Tran-Cong, Q.; Harada, A., Reaction-induced ordering phenomena in binary polymer mixtures. *Phys Rev Lett* **1996,** *76* (7), 1162-1165.

11. Matsen, M. W., Equilibrium behavior of asymmetric ABA triblock copolymer melts. *The Journal of Chemical Physics* **2000,** *113* (13).

12. Court, F. o.; Yamaguchi, D.; Hashimoto, T., Morphological and Scattering Studies of Binary Mixtures of Block Copolymers: Cosurfactant Effects Observed in the Parameter Space of Temperature, Blend Composition, and Molecular Weight Ratio. *Macromolecules* **2008,** *41* (13), 4828-4837.

13. Lee, J. H.; Koh, C. Y.; Singer, J. P.; Jeon, S. J.; Maldovan, M.; Stein, O.; Thomas, E. L., 25th anniversary article: ordered polymer structures for the engineering of photons and phonons. *Adv Mater* **2014,** *26* (4), 532-69.

14. Macfarlane, R. J.; Kim, B.; Lee, B.; Weitekamp, R. A.; Bates, C. M.; Lee, S. F.; Chang, A. B.; Delaney, K. T.; Fredrickson, G. H.; Atwater, H. A.; Grubbs, R. H., Improving brush polymer infrared one-dimensional photonic crystals via linear polymer additives. *J Am Chem Soc* **2014,** *136* (50), 17374-7.

15. Shi, W.; Fredrickson, G. H.; Kramer, E. J.; Ntaras, C.; Avgeropoulos, A.; Demassieux, Q.; Creton, C., Mechanics of an Asymmetric Hard-Soft Lamellar Nanomaterial. *ACS Nano* **2016,** *10* (2), 2054-62.

16. Shi, W.; Hamilton, A. L.; Delaney, K. T.; Fredrickson, G. H.; Kramer, E. J.; Ntaras, C.; Avgeropoulos, A.; Lynd, N. A., Creating Extremely Asymmetric Lamellar Structures via Fluctuation-Assisted Unbinding of Miktoarm Star Block Copolymer Alloys. *J Am Chem Soc* **2015,** *137* (19), 6160-3.

17. Shi, W.; Lynd, N. A.; Montarnal, D.; Luo, Y.; Fredrickson, G. H.; Kramer, E. J.; Ntaras, C.; Avgeropoulos, A.; Hexemer, A., Toward Strong Thermoplastic Elastomers with

Asymmetric Miktoarm Block Copolymer Architectures. *Macromolecules* **2014,** *47* (6), 2037-2043.

18. Huang, M.; Yue, K.; Huang, J.; Liu, C.; Zhou, Z.; Wang, J.; Wu, K.; Shan, W.; Shi, A. C.; Cheng, S. Z. D., Highly Asymmetric Phase Behaviors of Polyhedral Oligomeric Silsesquioxane-Based Multiheaded Giant Surfactants. *ACS Nano* **2018,** *12* (2), 1868-1877.

19. Watanabe, K.; Katsuhara, S.; Mamiya, H.; Kawamura, Y.; Yamamoto, T.; Tajima, K.; Isono, T.; Satoh, T., Highly asymmetric lamellar nanostructures from nanoparticle-linear hybrid block copolymers. *Nanoscale* **2020,** *12* (31), 16526-16534.

20. Court, F.; Hashimoto, T., Morphological Studies of Binary Mixtures of Block Copolymers. 1. Cosurfactant Effects and Composition Dependence of Morphology. *Macromolecules* **2001,** *34* (8), 2536-2545.

21. Court, F.; Yamaguchi, D.; Hashimoto, T., Morphological Studies of Binary Mixtures of Block Copolymers: Temperature Dependence of Cosurfactant Effects. *Macromolecules* **2006,** *39* (7), 2596-2605.

22. Shi, W.; Hamilton, A. L.; Delaney, K. T.; Fredrickson, G. H.; Kramer, E. J.; Ntaras, C.; Avgeropoulos, A.; Lynd, N. A., Creating Extremely Asymmetric Lamellar Structures via Fluctuation-Assisted Unbinding of Miktoarm Star Block Copolymer Alloys. *Journal of the American Chemical Society* **2015,** *137* (19), 6160-6163.

23. Lequieu, J.; Magenau, A. J. D., Reaction-induced phase transitions with block copolymers in solution and bulk. *Polymer Chemistry* **2021,** *12* (1), 12-28.

24. Lee, K.; Corrigan, N.; Boyer, C., Polymerization Induced Microphase Separation for the Fabrication of Nanostructured Materials. *Angew Chem Int Ed Engl* **2023,** *62* (44), e202307329.

25. Oh, T.; Cho, S.; Yoo, C.; Yeo, W.; Oh, J.; Seo, M., Polymerization-induced microphase separation of a polymerization mixture into nanostructured block polymer materials. *Progress in Polymer Science* **2023,** *145*.

26. Fischer, M.; Hellmann, G. P., On the Evolution of Phase Patterns during the High-Impact-Modified Polystyrene Process. *Macromolecules* **1996,** *29* (7), 2498-2509.

27. Seo, M.; Hillmyer, M. A., Reticulated nanoporous polymers by controlled polymerization-induced microphase separation. *Science* **2012,** *336* (6087), 1422-5.

28. Park, J.; Saba, S. A.; Hillmyer, M. A.; Kang, D.-C.; Seo, M., Effect of homopolymer in polymerization-induced microphase separation process. *Polymer* **2017,** *126*, 338-351.

29. Mukai, M.; Sato, M.; Miyadai, W.; Maruo, S., On-Demand Tunability of Microphase Separation Structure of 3D Printing Material by Reversible Addition/Fragmentation Chain Transfer Polymerization. *Polymers (Basel)* **2023,** *15* (17).

30. Maruyama, T.; Mukai, M.; Sato, R.; Iijima, M.; Sato, M.; Furukawa, T.; Maruo, S., Multifunctional 3D Printing of Heterogeneous Polymer Structures by Laser-Scanning Micro-Stereolithography Using Reversible Addition–Fragmentation Chain-Transfer Polymerization. *ACS Applied Polymer Materials* **2022,** *4* (8), 5515-5523.

31. Shi, X.; Bobrin, V. A.; Yao, Y.; Zhang, J.; Corrigan, N.; Boyer, C., Designing Nanostructured 3D Printed Materials by Controlling Macromolecular Architecture. *Angew Chem Int Ed Engl* **2022,** *61* (35), e202206272.

32. Schulze, M. W.; Hillmyer, M. A., Tuning Mesoporosity in Cross-Linked Nanostructured Thermosets via Polymerization-Induced Microphase Separation. *Macromolecules* **2017,** *50* (3), 997-1007.

33. Motokawa, R.; Taniguchi, T.; Kumada, T.; Iida, Y.; Aoyagi, S.; Sasaki, Y.; Kohri, M.; Kishikawa, K., Photonic Crystals Fabricated by Block Copolymerization-Induced Microphase Separation. *Macromolecules* **2016,** *49* (16), 6041-6049.

34. Motokawa, R.; Iida, Y.; Zhao, Y.; Hashimoto, T.; Koizumi, S., Living Polymerization Induced Macro- and Microdomain Investigated by Focusing Ultra-small-angle Neutron Scattering. *Polymer Journal* **2007,** *39* (12), 1312-1318.

35. Zaremski, M. Y.; Kozhunova, E. Y.; Abramchuk, S. S.; Glavatskaya, M. E.; Chertovich, A. V., Polymerization-induced phase separation in gradient copolymers. *Mendeleev Communications* **2021,** *31* (2), 277-279.

36. Lalande, L.; Plummer, C. J. G.; Månson, J.-A. E.; Gérard, P., The influence of matrix modification on fracture mechanisms in rubber toughened polymethylmethacrylate. *Polymer* **2006,** *47* (7), 2389-2401.

37. Gerard, P.; Couvreur, L.; Magnet, S.; Ness, J.; Schmidt, S., Controlled Architecture Polymers at Arkema: Synthesis, Morphology and Properties of All-Acrylic Block Copolymers. In *Controlled/Living Radical Polymerization: Progress in RAFT, DT, NMP & OMRP*, 2009; pp 361-373.

38. Mori, Y.; Lim, L. S.; Bates, F. S., Consequences of Molecular Bridging in Lamellae-Forming Triblock/Pentablock Copolymer Blends. *Macromolecules* **2003,** *36* (26), 9879-9888.

39. Lynd, N. A.; Oyerokun, F. T.; O'Donoghue, D. L.; Handlin, D. L.; Fredrickson, G. H., Design of Soft and Strong Thermoplastic Elastomers Based on Nonlinear Block Copolymer Architectures Using Self-Consistent-Field Theory. *Macromolecules* **2010,** *43* (7), 3479-3486.

40. Dufour, B.; Koynov, K.; Pakula, T.; Matyjaszewski, K., PBA-PMMA 3-Arm Star Block Copolymer Thermoplastic Elastomers. *Macromolecular Chemistry and Physics* **2008,** *209* (16), 1686-1693.

41. Ishizu, K.; Uchida, S., Synthesis and microphase-separated structures of star-block copolymers. *Progress in Polymer Science* **1999,** *24* (10), 1439-1480.

42. Podzimek, S., *Light Scattering Size Exclusion Chromatography and Asymmetric Flow Field Flow Fractionation.* A John Wiley & Sons, Inc. : 2011.

43. Yamaguchi, D.; Hashimoto, T., A Phase Diagram for the Binary Blends of Nearly Symmetric Diblock Copolymers. 1. Parameter Space of Molecular Weight Ratio and Blend Composition. *Macromolecules* **2001,** *34* (18), 6495-6505.

44. Hashimoto, T.; Yamasaki, K.; Koizumi, S.; Hasegawa, H., Ordered Structure in Blends of Block Copolymers .1. Miscibility Criterion for Lamellar Block Copolymers. *Macromolecules* **1993,** *26* (11), 2895-2904.

45. Semenov, A. N., Theory of block copolymer interfaces in the strong segregation limit. *Macromolecules* **2002,** *26* (24), 6617-6621.

46. Semenov, A. N., Contribution to the Theory of Microphase Layering in Block-Copolymer Melts. *Zhurnal Eksperimentalnoi I Teoreticheskoi Fiziki* **1985,** *88* (4), 1242-1256.

47. Hashimoto, T.; Shibayama, M.; Kawai, H., Domain-Boundary Structure of Styrene-Isoprene Block Copolymer Films Cast from Solution. 4. Molecular-Weight Dependence of Lamellar Microdomains. *Macromolecules* **2002,** *13* (5), 1237-1247.

48. Matsushita, Y.; Takasu, T.; Yagi, K.; Tomioka, K.; Noda, I., Preparation and morphologies of 4- and 12-armed styrene-isoprene star-shaped block copolymers. *Polymer* **1994,** *35* (13), 2862-2866.

49. Hashimoto, T., Generalized view of molecular weight dependence of microdomain size of block polymers. Appraisal of Hadziioannou-Skoulios' data on binary mixtures of block polymers. *Macromolecules* **2002,** *15* (6), 1548-1553.